

MODEL-INDEPENDENT INSIGHTS INTO THE NATURE OF THE LY α FOREST AND THE DISTRIBUTION OF MATTER IN THE UNIVERSE

JOOP SCHAYE

School of Natural Sciences, Institute for Advanced Study, Einstein Drive, Princeton NJ 08540, schaye@ias.edu

Accepted for publication in the Astrophysical Journal

ABSTRACT

Straightforward physical arguments are used to derive the properties of Ly α forest absorbers. It is shown that many aspects of the current physical picture of the forest, in particular the fact that the absorption arises in extended structures of moderate overdensities which contain a large fraction of the baryons in the universe, can be derived directly from the observations without making any specific assumptions about the presence and distribution of dark matter, the values of the cosmological parameters or the mechanism for structure formation. The key argument is that along any line of sight intersecting a gravitationally confined gas cloud, the size of the region over which the density is of order the maximum density, is typically of order the local Jeans length. This is true for overdense absorbers, regardless of the shape of the cloud and regardless of whether the cloud as a whole is in dynamical equilibrium. The simple analytic model is used to derive the mass distribution of the photoionized gas directly from the observed column density distribution. It is demonstrated that the shape of the column density distribution, in particular the observed deviations from a single power-law, and its evolution with redshift, reflect the shape of the matter distribution and can be understood in terms of the growth of structure via gravitational instability in an expanding universe.

Subject headings: cosmology: theory — galaxies: formation — intergalactic medium — quasars: absorption lines — hydrodynamics

1. INTRODUCTION

The Ly α forest is thought to arise in the smoothly fluctuating intergalactic medium (IGM), which traces the distribution of the dark matter on large scales. Mildly overdense regions give rise to low column density absorption lines ($N_{HI} \lesssim 10^{14.5} \text{ cm}^{-2}$), whose widths are determined mainly by thermal broadening and the differential Hubble flow across the absorber. Although many aspects of this physical picture of the Ly α forest can already be found in papers by Bi, Börner, & Chu (1992) and Bi (1993), who used a semi-analytic model with a log-normal distribution for the dark matter; it gained acceptance only after it was confirmed and extended by hydrodynamical simulations (e.g., Cen et al. 1994; Zhang, Anninos, & Norman 1995; Hernquist et al. 1996; Miralda-Escudé et al. 1996; Theuns et al. 1998). In the simulations the Ly α forest arises in a network of sheets, filaments, and halos, which give rise to absorption lines of progressively higher column densities. This physical picture of the forest is supported by observations of gravitationally lensed quasars and quasar pairs, which show that the characteristic sizes of the absorbers are 10s to 100s of kpc (e.g., Bechtold et al. 1994; Dinshaw et al. 1994, 1995; Smette et al. 1995) and by the success of cosmological simulations in reproducing the statistics of the observed absorption spectra (see Efstathiou, Schaye, & Theuns 2000 for a recent review).

Following Rees (1986), most theoretical work on the Ly α forest has been carried out within the framework of the cold dark matter paradigm. In virtually every case an ab-initio approach was followed, i.e. the properties of the forest were predicted for a particular model of structure formation and then compared to observations (but see for example Weinberg et al. 1997 and Nusser & Haehnelt 1999 for notable exceptions). The models, which can be either semi-analytic or fully numerical, are specified by the cosmological parameters, the initial power spectrum, and the evolution of the UV background radiation.

In this paper a rather different approach will be taken. It will be shown that many properties of the absorbers, including their densities and radial sizes, can be derived using straightforward physical arguments, independent of the details of the cosmological model. The key physical argument is that the absorbers will generally not be far from local hydrostatic equilibrium, i.e. the size of the region over which the density is of order the maximum density along the sightline, is of order the local Jeans length. It will be argued that this is very likely the case for overdense absorbers, regardless of whether the cloud as a whole is in hydrostatic equilibrium. The same formalism will be used to explain the observed structure in the column density distribution and to derive the density distribution of the photoionized IGM directly from the observations.

The main physical arguments underlying this work are presented in section 2. Although the expressions derived in section 2 apply to all gravitationally confined gas clouds, only photoionized, optically thin clouds ($N_{HI} \lesssim 10^{17} \text{ cm}^{-2}$) are discussed in subsequent sections. The properties of self-shielded clouds, which are relevant for protogalactic clumps, Lyman limit systems, and damped Ly α absorbers, are derived in Schaye (2001). The formalism of section 2 is used to derive the physical properties of Ly α forest absorbers in section 3. The cosmological implications of the observed column density distribution are discussed in section 4. Finally, the main conclusions are summarized in section 5. Throughout the paper, numerical values will be inserted for physical parameters whose values are thought to be well known. The full expressions can be found in the appendix.

2. HYDRODYNAMICS

In this section the physical properties of self-gravitating gas clouds will be derived. It will be argued that along each sightline through an overdense absorber, the sound crossing timescale t_{sc} , is of order the local dynamical timescale t_{dyn} . In

other words, the characteristic size of the absorber is typically of order the local Jeans length. The characteristic size is defined as the size of the region for which the density is of order the characteristic density of the absorber. In section 2.1 it will be shown that because most of the absorption takes place in the densest gas along the sightline, a well-defined characteristic density does exist.

Consider a cloud with characteristic density n_H . The dynamical (or free-fall) time is

$$t_{\text{dyn}} \equiv \frac{1}{\sqrt{G\rho}} \sim 1.0 \times 10^{15} \text{ s} \left(\frac{n_H}{1 \text{ cm}^{-3}} \right)^{-1/2} \left(\frac{1-Y}{0.76} \right)^{1/2} \left(\frac{f_g}{0.16} \right)^{1/2}, \quad (1)$$

where f_g is fraction of the mass in gas¹ and Y is the baryonic mass fraction in helium, which will be set equal to 0.24 hereafter. In cold, collapsed clumps f_g could be close to unity, but on the scales of interest here f_g will not be far from its universal value, $f_g \approx \Omega_b/\Omega_m$. Let L be the characteristic size of the cloud, i.e. the length of the intersected part of the cloud over which the density is of order the characteristic density. The sound crossing time is then

$$t_{\text{sc}} \equiv \frac{L}{c_s} \sim 2.0 \times 10^{15} \text{ s} \left(\frac{L}{1 \text{ kpc}} \right) T_4^{-1/2} \left(\frac{\mu}{0.59} \right)^{1/2}, \quad (2)$$

where c_s is the sound speed in an ideal, monatomic gas with the ratio of specific heats $\gamma = 5/3$, $T \equiv T_4 \times 10^4 \text{ K}$, and μ is the mean molecular weight. In what follows μ will be set equal to the value appropriate for a fully ionized, primordial plasma, $\mu = 4/(8-5Y) \approx 0.59$.

The equation for hydrostatic equilibrium is $dP/dr = -G\rho M/r^2$, where M is the mass interior to r . Since the pressure $P \sim c_s^2 \rho$, this implies $c_s^2 \rho/L \sim G\rho^2 L$, i.e. $t_{\text{sc}} \sim t_{\text{dyn}}$. There are many other ways of showing that in hydrostatic equilibrium $t_{\text{sc}} \sim t_{\text{dyn}}$. It can for example readily be seen that it implies that the sound speed is of order the circular velocity. The condition $t_{\text{sc}} = t_{\text{dyn}}$ defines a characteristic length, the so-called Jeans length²,

$$L_J \equiv \frac{c_s}{\sqrt{G\rho}} \sim 0.52 \text{ kpc} n_H^{-1/2} T_4^{1/2} \left(\frac{f_g}{0.16} \right)^{1/2}. \quad (3)$$

To make a connection with observations, it is useful to introduce the ‘Jeans column density’,

$$N_{H,J} \equiv n_H L_J \sim 1.6 \times 10^{21} \text{ cm}^{-2} n_H^{1/2} T_4^{1/2} \left(\frac{f_g}{0.16} \right)^{1/2}, \quad (4)$$

If $t_{\text{sc}} \gg t_{\text{dyn}}$, then the cloud is Jeans unstable and will either fragment or, since $v \sim L/t_{\text{dyn}} \gg c_s$, shock to the virial temperature. In either case, equilibrium will be restored on the dynamical timescale. If, on the other hand, $t_{\text{sc}} \ll t_{\text{dyn}}$, then the cloud will expand or evaporate and equilibrium will be restored on the sound crossing timescale.

Although the Jeans criterion for gravitational instability is familiar, it is not always appreciated that a growing density perturbation will generally be close to ‘local hydrostatic equilibrium’, i.e. $t_{\text{sc}} \sim t_{\text{dyn}}$ locally, but not necessarily for the cloud as a whole. In other words, along any sightline through the evolving cloud, which will in general not be spherical, the length

of the region for which the density is of order the maximum density, will be of order the local Jeans length. If the cloud has substructure, then the condition of local hydrostatic equilibrium should be applied to each density maximum along the sightline. Note that the concept of a Jeans mass only makes sense if the cloud is roughly spherical. The collapse will in general not be synchronized along all three spatial dimensions, and a density perturbation may first collapse into a sheet-like or filamentary structure before reaching a more spheroidal configuration. Furthermore, the tidal field around collapsed regions can induce the formation of a network of sheets and filaments. Although the mass of the region containing the perturbation can thus differ substantially from the Jeans mass, *along any sightline intersecting an evolving perturbation, the characteristic size will generally be of order the local Jeans length.*

Large departures from local hydrostatic equilibrium do occur when the pressure changes on a timescale much shorter than t_{dyn} . For example, during shell crossing the density suddenly increases by a large factor. This will result in shocks, leading to virialization and equilibrium will quickly be restored. A sudden drop in the temperature through a thermal instability is another example. In that case equilibrium will be restored through fragmentation. These two examples are relevant for high column density absorbers and are discussed in more detail in Schaye (2001). For the Ly α forest, sudden heating is in fact more relevant. During reionization the temperature of the diffuse IGM is suddenly raised by several orders of magnitude to at least 10^4 K and possibly $\gtrsim 10^5 \text{ K}$, depending on the speed of reionization and the spectrum of the ionizing radiation. Because of the sudden increase in the Jeans length during reionization, $t_{\text{sc}} \ll t_{\text{dyn}}$ for most of the gas. Until pressure forces have had time to restore local hydrostatic equilibrium, the gas can be clumpy on scales smaller than the Jeans length (e.g., Gnedin & Hui 1998). Simulations by Gnedin (2000) show that even if the IGM was reionized as late as $z \sim 7$, the baryon smoothing scale is again similar to the Jeans scale by the redshifts of interest here ($z \leq 4$).

Pressure forces can only smooth the gas distribution on scales smaller than the sound horizon, which is defined by the condition $t_{\text{sc}} \sim H^{-1}$. Hydrostatic equilibrium would then require $t_{\text{dyn}} \sim H^{-1}$, which implies $\rho \sim \bar{\rho}$. Hence, the assumption of local hydrostatic equilibrium may break down for absorbers with characteristic densities smaller than the cosmic mean. The precise value of the sound horizon depends on the thermal history of the IGM. After reionization, the temperature of the low-density IGM is expected to drop. At very high redshift ($z \gtrsim 7$) the IGM can cool efficiently through inverse Compton scattering off the microwave background, but after that the main cooling mechanism is adiabatic expansion and the cooling time is thus of order the Hubble time. Hence, for $z < z_{\text{reion}}$, the sound horizon is greater than c_s/H , which implies that the statement that local hydrostatic equilibrium is only a good approximation for overdense absorbers, is conservative.

Finally, if a cloud is not gravitationally supported, then local hydrostatic equilibrium does not necessarily imply that its characteristic size is of order the local Jeans length. A cloud that is not supported by self-gravity can be pressure confined, rotationally supported or it can be not supported at all. Although pressure confinement may be important for the high column density absorption lines, the possibility that a significant frac-

¹Stars and molecules do *not* contribute to f_g .

²The Jeans length or, equivalently, the dynamical timescale is not well defined and some authors include a dimensionless coefficient of order unity in the definition. However, the value of the dimensionless coefficient depends on the geometry of the cloud and it is hard to justify any particular choice.

tion of the Ly α forest arises in pressure confined clouds has been ruled out on both observational and theoretical grounds (e.g., Rauch 1998). Even if every Ly α absorption line were to arise in a rotationally supported cloud, then the characteristic size will only be much greater than the Jeans length for sightlines that are nearly perpendicular to the spin axis of the cloud, which cannot be true for a large fraction of the absorption lines. As discussed above, unless the cloud is kept in a steady state by external pressure or by a centrifugal barrier, local hydrostatic equilibrium is restored on a timescale $t \ll H^{-1}$ if the absorber is overdense. Hence, if a population of Ly α forest absorbers exists that are quasi-stable, i.e. whose lifetimes are not much shorter than the Hubble time, then any given absorption line is unlikely to arise in a transient cloud, i.e. a cloud with a lifetime $t \ll H^{-1}$, unless most of the matter in the universe is contained in clouds far from dynamical equilibrium. In summary, it is very likely that local hydrostatic equilibrium is a good approximation for most Ly α forest absorbers.

2.1. The characteristic density

The characteristic density is the column density weighted density of an absorber. It is easily demonstrated that for a wide range of density profiles, the neutral hydrogen column density through a cloud is dominated by the region with the highest density. For a spherical cloud with a density profile $n_H \propto r^{-n}$, the neutral hydrogen column density in a sightline with impact parameter b is

$$N_{HI} \propto \int_{-\infty}^{+\infty} (b^2 + l^2)^{-n} l dl, \quad (5)$$

where I used the fact that the neutral fraction in an optically thin gas is proportional to the density. For $n > 1/2$, the dominant contribution to the column density comes from $l \lesssim b$ and $N_{HI} \sim n_{HI}(b)b$. For example, for a singular isothermal sphere ($n = 2$), the column density weighted density is $\langle n_H \rangle \equiv \int n_H n_{HI} dl / \int n_{HI} dl = \frac{3}{4} n_H(b)$. Hence, for reasonable density profiles, almost all the absorption takes place in the densest part of the gas cloud. This implies the existence of a characteristic density, which will be close to the maximum density along the line of sight through the cloud.

3. PHYSICAL PROPERTIES

In the previous section expressions were derived for the size and total hydrogen column density of an absorber as a function of its density and temperature. To make contact with observations it is necessary to compute the neutral fraction since it is the neutral hydrogen column density that is observed. Here, only optically thin clouds ($N_{HI} \lesssim 10^{17} \text{ cm}^{-2}$) will be considered, for which the ionization correction can be computed analytically.

The neutral fraction of a highly ionized, optically thin gas is

$$\frac{n_{HI}}{n_H} = n_e \beta_{HII} \Gamma^{-1} \sim 0.46 n_H T_4^{-0.76} \Gamma_{12}^{-1}, \quad (6)$$

where $\beta_{HII} \approx 4 \times 10^{-13} T_4^{-0.76} \text{ cm}^3 \text{ s}^{-1}$ and $\Gamma \equiv \Gamma_{12} \times 10^{-12} \text{ s}^{-1}$ are the hydrogen recombination and photoionization rates respectively and n_e is the number density of free electrons. The photoionization rate corresponding to a UV background intensity of $J(\nu) \text{ erg s}^{-1} \text{ cm}^{-2} \text{ sr}^{-1} \text{ Hz}^{-1}$ is

$$\Gamma = \int_{\nu_L}^{\infty} \frac{4\pi J(\nu) \sigma(\nu)}{h\nu} d\nu, \quad (7)$$

³The cooling time depends on the neutral fraction and thus on Γ . If $\Gamma_{12} \ll 1$, as is the case at low redshift, then atomic cooling will become efficient at much lower densities than 10^{-4} cm^{-3} .

where σ is the cross section for photoionization and ν_L is the frequency at the Lyman limit. At redshifts $2 \lesssim z \lesssim 4$, studies of the proximity effect find $\Gamma \sim 10^{-12} \text{ s}^{-1}$ with a relative uncertainty of order unity (Scott et al. 2000 and references therein), which is in reasonable agreement with models of the UV background from quasars (e.g., Haardt & Madau 1996). At low redshift ($z \lesssim 0.5$) the intensity of the UV background is thought to be considerably lower, $\Gamma \approx 10^{-14} - 10^{-13} \text{ s}^{-1}$ (e.g., Davé & Tripp 2001 and references therein).

To make further progress, an estimate of the temperature is needed. It has been known since long that the widths of Ly α absorption lines are consistent with photoionization temperatures, $T \sim 10^4 \text{ K}$ (e.g., Carswell et al. 1984). Gas with a temperature significantly lower than this is heated on the photoionization timescale, $t = \Gamma^{-1} \ll H^{-1}$. To reach temperatures $T \gg 10^4 \text{ K}$, the gas would have to be shock-heated. Accretion shocks associated with gravitational collapse are likely to be important only for gas at high overdensities, but galactic winds could in principle heat a large fraction of the IGM. For densities $n_H \gtrsim 10^{-4} \text{ cm}^{-3}$ ($\delta \gtrsim 10$ at $z \sim 3$), atomic cooling is efficient³ and the temperature will be approximately 10^4 K (molecular cooling can lead to lower temperatures, but the molecular fraction is negligible for optically thin clouds). Cooling can become inefficient if the temperature is very high, $T \gg 10^5 \text{ K}$, but in that case collisional ionization suppresses the neutral fraction and the gas will only give rise to lines of very low column density. In short, $T \sim 10^4$ is likely to be a good approximation for the Ly α forest, although a somewhat higher temperature could be appropriate at $n_H \lesssim 10^{-4} \text{ cm}^{-3}$ if galactic winds are important.

3.1. Densities

Substituting equation 6 into equation 4 yields a relation between the neutral hydrogen column density and the characteristic density,

$$N_{HI} \sim 2.3 \times 10^{13} \text{ cm}^{-2} \left(\frac{n_H}{10^{-5} \text{ cm}^{-3}} \right)^{3/2} T_4^{-0.26} \Gamma_{12}^{-1} \left(\frac{f_g}{0.16} \right)^{1/2}. \quad (8)$$

Because the gas responsible for the low-column density Ly α forest is still expanding, it is often instructive to use the density contrast, $\delta \equiv (n_H - \bar{n}_H) / \bar{n}_H$, where

$$\bar{n}_H \approx 1.1 \times 10^{-5} \text{ cm}^{-3} \left(\frac{1+z}{4} \right)^3 \left(\frac{\Omega_b h^2}{0.02} \right), \quad (9)$$

instead of n_H ,

$$N_{HI} \sim 2.7 \times 10^{13} \text{ cm}^{-2} (1+\delta)^{3/2} T_4^{-0.26} \Gamma_{12}^{-1} \left(\frac{1+z}{4} \right)^{9/2} \left(\frac{\Omega_b h^2}{0.02} \right)^{3/2} \left(\frac{f_g}{0.16} \right)^{1/2}. \quad (10)$$

Clearly, the low-column density Ly α forest arises in gas of low overdensity. Virialized minihalos have $\delta \gtrsim 10^2$ which corresponds to high column density absorption lines, $N_{HI} > 10^{16} \text{ cm}^{-2}$ at $z \sim 3$. The presence of dark matter does not have

a dramatic effect on the inferred densities: if $f_g = 1$ instead of 0.16 ($\approx \Omega_b/\Omega_m$), then the density contrast corresponding to a fixed column density is only about a factor 2 smaller.

The neutral hydrogen column density corresponding to a fixed density contrast is about a factor $5 \times 10^2 \Gamma(z=0)/\Gamma(z=3) \sim 5\text{--}50$ lower at $z \sim 0$ than at $z \sim 3$, with only a weak dependence on the evolution of the temperature. Because the strong dependence on redshift is partially offset by the evolution of Γ , the local Ly α forest is not fundamentally different from the $z \sim 3$ forest.

Hydrodynamical simulations have been used to make detailed predictions for the low column density Ly α forest. Although the formalism developed here does not make any specific assumptions about the cosmology or the nature of the dark matter, it can of course be applied to the specific models tested with the simulations. In the simulations (which generally do not include feedback from star formation or radiative transfer effects) it is found that the low-density gas ($n_H \lesssim 10^{-4} \text{ cm}^{-3}$, $\delta \lesssim 10$ at $z \sim 3$) follows a tight temperature-density relation, which can be approximated by a power-law, $T = T_0(1+\delta)^\alpha$ (Hui & Gnedin 1997). Substituting this relation into equation 10 yields,

$$N_{HI} \sim 2.7 \times 10^{13} \text{ cm}^{-2} (1+\delta)^{1.5-0.26\alpha} T_{0.4}^{-0.26} \Gamma_{12}^{-1} \left(\frac{1+z}{4}\right)^{9/2} \left(\frac{\Omega_b h^2}{0.02}\right)^{3/2} \left(\frac{f_g}{0.16}\right)^{1/2} \quad (11)$$

$$(n_H \lesssim 10^{-4} \text{ cm}^{-3}).$$

From comparisons of the line widths in simulated and observed spectra it is found that $T_0 \sim 2 \times 10^4 \text{ K}$ and $\alpha \sim 0.0\text{--}0.3$ at $z \sim 3$ (e.g., Schaye et al. 2000; McDonald et al. 2001).

Davé et al. (1999, hereafter DHKW) find that the following empirical relation fits the results of their simulation over the range $z = 0\text{--}3$: $N_{HI} \sim 10^{14} \text{ cm}^{-2} \left[\frac{1}{20}(1+\delta)10^{0.4z}\right]^{1/0.7}$, although the scatter is large for $z \lesssim 1$. This relation is of course specific to the simulation of DHKW, i.e. it would have been different if they had used a simulation with a different cosmology, UV background or temperature. Nevertheless, we can compare it to equation 11 if we set all the other parameters to the values of DHKW's simulation⁴. The normalization ($N_{HI}(\delta = 0)$) of DHKW turns out to be about a factor 3 higher (7.2×10^{13} vs. 2.3×10^{13}), which is about as good as could be expected considering that there is an uncertainty of order unity in the normalization of both equation 11 (because of some arbitrariness in the value of the dimensionless coefficient in the definition of the Jeans length) and the empirical relation of DHKW (because of the arbitrariness in the definition of the density contrast corresponding to an absorption line in a simulated spectrum). In fact, the normalizations found by different groups vary by about an order of magnitude, with most groups finding somewhat lower values for $N_{HI}(\delta = 0)$ than DHKW (e.g., Bryan et al. 1999; Schaye et al. 1999). Equation 11 also reproduces the scaling of N_{HI} with δ and z remarkably well. DHKW find $N_{HI} \propto (1+\delta)^{1.43}$, whereas equation 11 gives $N_{HI} \propto (1+\delta)^{1.37}$ for the value of α found by DHKW ($\alpha \approx 0.5$). In the simulation of DHKW, $N_{HI}(z=3)/N_{HI}(z=2) \approx 3.7$ and $N_{HI}(z=2)/N_{HI}(z=0) \approx 6.3$, while equation 11 yields values of 5.1 and 4.1, assuming that Γ evolves according to the model of Haardt & Madau (1996), which was used by DHKW, and a constant temperature. In

summary, equation 11 matches the results produced by hydrodynamical simulations very well.

3.2. Radial sizes

The radial sizes of absorbers can be expressed as a function of their neutral hydrogen column densities by combining equations 3, 6, and 8,

$$L \sim 1.0 \times 10^2 \text{ kpc} \left(\frac{N_{HI}}{10^{14} \text{ cm}^{-2}}\right)^{-1/3} T_4^{0.41} \Gamma_{12}^{-1/3} \left(\frac{f_g}{0.16}\right)^{2/3} \quad (12)$$

Hence, Ly α forest absorbers are large, $L \sim 10^2 \text{ kpc}$, with only a weak dependence on the column density, temperature, and ionizing background. Even clouds of $N_{HI} \sim 10^{17} \text{ cm}^{-2}$, the highest column density for which self-shielding can be neglected, have a characteristic size of 10 kpc.

Equation 12 shows that the physical size of an absorber of a fixed neutral hydrogen column density does not depend explicitly on redshift. The main time dependence comes from the dependence on the ionization rate, which is thought to peak in the range $z \sim 2\text{--}3$. From redshift $z \sim 3$ to 0 the ionization rate probably decreases by a factor 10–30, which implies that the physical sizes of $z \sim 0$ absorbers are about a factor 2 to 3 greater than those of $z \sim 3$ absorbers with the same N_{HI} . The comoving sizes, however, are smaller at $z \sim 0$ than at $z \sim 3$ by a factor 4/3 to 2.

If the absorber has not decoupled from the Hubble expansion, then the differential Hubble flow across the absorber broadens the absorption line, leading to a Hubble width of $b_H \sim H(z)L/2$, where H is the Hubble parameter. The Hubble width is comparable to the thermal width, $b_T \equiv \sqrt{2kT/m} \approx 12.8 T_4^{1/2} \text{ km s}^{-1}$, for $N_{HI} \sim 10^{13}\text{--}10^{14} \text{ cm}^{-2}$. In reality, absorbers are not expanding freely and peculiar velocity gradients will change the redshift space sizes of the absorbers. Note, however, that peculiar velocity gradients cannot decrease the width of a line below the thermal width. The minimum line width as a function of the column density can therefore be used to measure the temperature as a function of the density (Schaye et al. 1999; Ricotti, Gnedin, & Shull 2000; Bryan & Machacek 2000). Finally, it is worth noting that the Hubble width increases almost as rapidly with temperature as the thermal broadening width, $b_H \propto T^{0.41}$ compared to $b_T \propto T^{0.5}$.

It is easily demonstrated that $b_H \sim b_T$ for a density contrast $\delta \sim 0$: since $c_s \sim b_T$ and $t_{\text{dyn}} \sim 1/H$, hydrostatic equilibrium implies $b_H \sim HL \sim Hc_s/t_{\text{dyn}} \sim b_T$. Similarly, it follows that for underdense absorbers $c_s < b_H$, i.e. sound waves cannot overcome the differential Hubble expansion across the absorber. This is just another way of showing that the fundamental assumption underlying this work, namely that the gas clouds will typically not be far from local hydrostatic equilibrium, breaks down for underdense absorbers.

Equations 10 and 12 predict the existence of a population of low column density ($N_{HI} \lesssim 10^{13} \text{ cm}^{-2}$ at $z \sim 3$) absorption lines that arise in underdense gas and are predominantly Hubble broadened. They should be broad and shallow and their profiles should deviate substantially from thermal profiles. Their characteristic sizes are greater than the sound horizon ($\Delta v \sim 10^2 \text{ km s}^{-1}$), which implies that the formalism developed in this paper is not well-suited to describe them. These lines trace the underlying matter distribution and can be regarded as a

⁴The simulation of DHKW has $\Omega_b h^2 = 0.02$, $\Omega_b/\Omega_m = 0.12$ ($= f_b$), $(T_{0.4}, \alpha) \approx (1.0, 0.5)$ at $z = 3$. They use the model of Haardt & Madau (1996) for the evolution of the ionizing background, but multiply the ionization rate by a factor 1.34.

“fluctuating Gunn-Peterson effect”. This means that large-scale correlations in the Ly α absorption can be used to constrain the primordial power spectrum (Croft et al. 1998).

3.3. Masses

If the absorbers are spherical, then their characteristic mass is $M_J \equiv \rho L^3$. Hence, the characteristic mass in gas is,

$$M_g \sim 8.8 \times 10^8 M_\odot \left(\frac{N_{HI}}{10^{14} \text{ cm}^{-2}} \right)^{-1/3} T_4^{1.41} \Gamma_{12}^{-1/3} \left(\frac{f_g}{0.16} \right)^{5/3}, \quad (13)$$

and the total mass is a factor $1/f_g$ higher. Of course, the absorbers may very well be far from spherical, in which case they can have masses very different from equation 13. Indeed, one would not expect mildly overdense regions, $\delta \lesssim 10$, to be spherical, as the collapse will generally not be synchronized along all three spatial dimensions. According to equation 10, such regions will give rise to absorption lines with column densities $N_{HI} \lesssim 10^{15} \text{ cm}^{-2}$ at $z \sim 3$.

4. COSMOLOGICAL IMPLICATIONS

From the observed incidence of absorption lines one can compute the total mass in neutral hydrogen, Ω_{HI} , by integrating over the column density distribution. Similarly, if the ionization correction is known, then the total baryon density in photoionized gas can be computed. Furthermore, the distribution of mass as a function of density can be derived from the differential column density distribution. The results obtained in the previous section make it possible to do this since equations 6 and 8 can be combined to yield the neutral fraction as a function of the neutral hydrogen column density.

4.1. Contribution to Ω_b

The mean gas density relative to the critical density can be obtained from the neutral hydrogen column density distribution,

$$\Omega_g = \frac{8\pi G m_H}{3H_0 c(1-Y)} \int N_{HI} \frac{n_H}{n_{HI}} f(N_{HI}, z) dN_{HI}, \quad (14)$$

where $f(N_{HI}, z)$ is the number density of absorption lines per unit absorption distance X (a dimensionless quantity defined by equation 15 below), and per unit column density. Observational results are usually expressed in terms of this function. Its relation to the quantity that is actually observed, the number density per unit redshift, dn/dz , depends on the assumed cosmology:

$$f(N_{HI}, z) \equiv \frac{d^2 n}{dN_{HI} dX} \equiv \frac{d^2 n}{dN_{HI} dz} \frac{H(z)}{H_0} \frac{1}{(1+z)^2}. \quad (15)$$

Combining equations 6, 8 and 14 yields

$$\Omega_g \sim 2.2 \times 10^{-9} h^{-1} \Gamma_{12}^{1/3} \left(\frac{f_g}{0.16} \right)^{1/3} T_4^{0.59} \int N_{HI}^{1/3} f(N_{HI}, z) dN_{HI}, \quad (16)$$

where $h \equiv H_0/(100 \text{ km s}^{-1} \text{ Mpc}^{-1})$. If the gas is not isothermal, then T will depend on N_{HI} and should therefore be moved inside the integral. Note that if $f_g = \Omega_b/\Omega_m$, then equation 16 agrees with the scaling relation familiar from the fluctuating Gunn-Peterson approximation, $\Omega_g \propto \Gamma^{1/2} h^{-3/2}$ (e.g., Rauch et al. 1997).

Observations indicate that at high redshift the column density distribution can be fit by a power-law, $f = BN_{HI}^{-\beta}$ with

$\beta \approx 1.5$, over a wide range of column densities (Tytler 1987). The fact that a single power-law appears to be a reasonable approximation is clear from Figure 1, which shows the observed distribution at $z \approx 2.8$. Hu et al. (1995) find that their data (solid points in Figure 1) is best fitted by a power-law with $B = 5.3 \times 10^7$ and $\beta = 1.46$ (for $(\Omega_m, \Omega_\Lambda) = (0.3, 0.7)$), and similar values are reported by others (e.g., Kirkman & Tytler 1997). This fit is shown as the dashed line in Figure 1. Assuming $(T_4, \Gamma_{12}, f_g, h) = (2.0, 1.0, 0.16, 0.65)$, equation 16 gives $\Omega_g h^2 (\log N_{HI} = 13-17.2) \approx 0.015$. Comparing this to the value derived from high redshift observations of the deuterium abundance, $\Omega_b h^2 \approx 0.020$ (O’Meara et al. 2001), we see that this leaves little room for stars, collisionally ionized gas, and gas in absorbers with $\log N_{HI} < 13$ or $\log N_{HI} > 17.2$. Clearly, a large fraction of the baryons reside in the Ly α forest.

It is important to note that it was implicitly assumed that the measured column densities of the absorption lines are similar to the true column densities. This assumption may, however, be incorrect for low column density lines. Observationally, the column density distribution is determined by decomposing absorption spectra into sets of Voigt profiles. In high-resolution spectra with a high signal-to-noise ratio, multiple Voigt components are usually required to obtain a satisfactory fit for a single absorption line. Low column density components are often placed in the wings of absorption lines. If these spurious lines were to dominate the column density distribution below some value of N_{HI} , then it would not be possible to use that part of the distribution to estimate the baryon density.

Another, related problem is that Monte Carlo simulations are often used to “correct” the observed column density distributions for the fraction of low column density lines that are thought to be “missing” because they are heavily blended with stronger lines. This procedure can result in an unphysical extension of the power-law distribution to arbitrary low column densities. In high quality spectra these corrections become important below $N_{HI} \sim 10^{13} \text{ cm}^{-2}$ at $z \sim 3$ (e.g., Hu et al. 1995). The data points shown in Figure 1 indicate the observed distribution, the “corrected” Hu et al. points would all fall on the dashed line. Unless current estimates of the baryon density are significantly in error, the distribution of column densities of *real* absorption lines, i.e. excluding Voigt components in the wings of absorption lines, cannot extend to much lower column densities.

Finally, it has to be kept in mind that the value obtained for Ω_g is uncertain to a factor of order unity because of the uncertainties in the values assumed for the various parameters and because of the fact that there is some arbitrariness in the value of the dimensionless coefficient in the definition of the Jeans length. These uncertainties do, however, not affect the derived scaling relations and the shape of the mass distribution, which is the subject of the next section.

4.2. Mass distribution

It is interesting to look at the differential distribution of the baryon density. If $f(N_{HI}, z) \propto N_{HI}^{-\beta}$, then equation 16 implies $\Omega_b \propto \int N_{HI}^{4/3-\beta} d \ln N_{HI}$. Hence, if $\beta < 4/3$, then the mass per decade of column density is an increasing function of N_{HI} and similarly, since $d \ln N_{HI} \propto d \ln n_H$ (equation 8), the mass per decade of density is an increasing function of n_H . There is evidence for deviations from a single power-law, the column density distribution seems to steepen somewhat

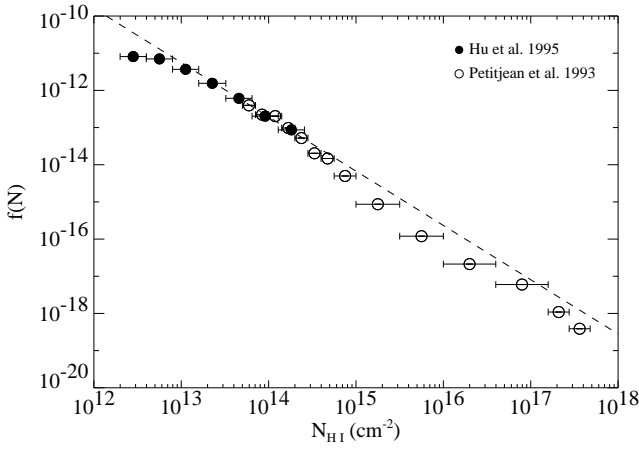


FIG. 1.— Observed neutral hydrogen column density distribution. Solid points are from Hu et al. (1995), *not* “corrected” for incompleteness; open circles are taken from the compilation by Petitjean et al. (1993). The dashed line is the power-law fit given by Hu et al., which is the best fit to their “corrected” data in the regime 2×10^{12} – 3×10^{14} cm^{-2} , $f(N_{\text{HI}}) = 5.3 \times 10^7 N_{\text{HI}}^{-1.46}$ (the normalization has been modified to that corresponding to a LCDM universe, $(\Omega_m, \Omega_\Lambda) = (0.3, 0.7)$). The mean redshift of both samples is 2.8.

above 10^{14} cm^{-2} (Kim et al. 1997) before flattening to $\beta \approx 1.32$ at $N_{\text{HI}} \gtrsim 10^{16}$ cm^{-2} (Petitjean et al. 1993). These trends are visible in Figure 1, although they are somewhat difficult to see in a log-log plot of $f(N_{\text{HI}})$ (they would have been more apparent if, contrary to convention, the quantity $\frac{d^2n}{d \log N_{\text{HI}} dX}$ had been plotted

instead of $\frac{d^2n}{dN_{\text{HI}} dX}$). Although the reality of the deviations from the single power-law is well established, their physical origin is not understood. In this section it will be shown that the shape of the column density distribution reflects the shape of the mass-weighted probability density distribution for the gas density, i.e. the mass distribution of the gas as a function of its density.

The mass distribution of the photoionized gas, $d\Omega_g/d \log(1+\delta)$, can be derived from the observed column density distribution using equations 10 and 16. The results for the data points shown in Figure 1 are plotted in Figure 2. The data points were computed using the same parameter values as were used in the previous section. Points corresponding to underdense gas ($\delta < 0$) are less reliable because the assumption of local hydrostatic equilibrium may break down, as was discussed before. Furthermore, the corresponding column densities are so low ($N_{\text{HI}} < 10^{13}$ cm^{-2} , column densities are indicated on the top axis of Figure 2) that many lines may have been lost in the noise. The two highest density data points are less reliable because the effect of self-shielding is no longer negligible. From equation 16 it can be seen that all points are proportional to the quantity $h^{-1} \Gamma_{12}^{1/3} f_g^{1/3} T_4^{0.59}$. Changing this quantity (or adding a dimensionless coefficient in the definition of the Jeans length) is equivalent to shifting the distribution vertically, but does not change the shape of the distribution.

In calculating $d\Omega_g/d \log(1+\delta)$ from $f(N_{\text{HI}})$, both the gas fraction f_g and the temperature T were assumed to be independent of N_{HI} . Hence, the shape of the distribution shown in Figure 2 is determined by the shape of the column density distribution. If the latter had been a strict power-law with spectral index β , then the former would also have been a power-law, but with index $4/3 - \beta$. Hence, the shape of the matter distribution function traces the deviations from the single power-law in

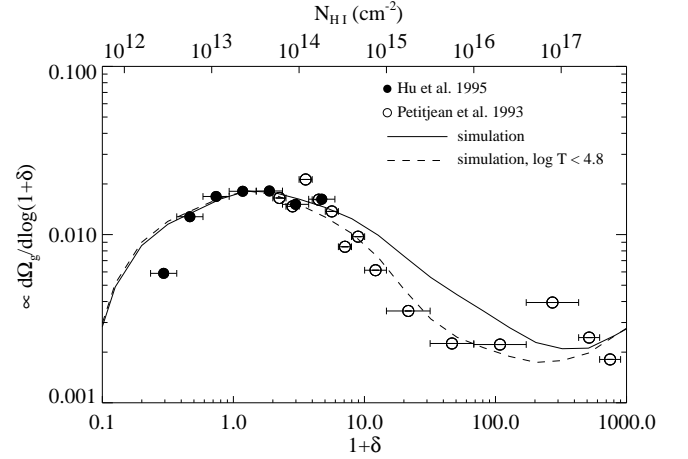


FIG. 2.— Mass distribution of photoionized gas. Data points are computed from the observed column density distribution and equation 16, using the same parameter values as were used in section 4.1: $(T_4, \Gamma_{12}, f_g, h, \Omega_m, \Omega_\Lambda) = (2.0, 1.0, 0.16, 0.65, 0.3, 0.7)$. The solid line indicates the mass distribution of all the gas in a hydrodynamical simulation at $z = 2.75$, the dashed line denotes the distribution of the gas that has a temperature $\log T < 4.8$. The curves have been normalized to have the same maximum as the Hu et al. (1995) points. The shape of the derived mass distribution suggests that gravitational instability is responsible for the growth of structure. The fall-off at $\delta \sim 10$ ($\log N_{\text{HI}} \sim 14.5$) can then be attributed to the onset of rapid, non-linear collapse and the flattening at $\delta \sim 10^2$ ($\log N_{\text{HI}} \sim 10^{16}$) to virialization. The shape of the distribution agrees well with the shape of the gas distribution in the hydrodynamical simulation (solid curve), in particular if hot gas, for which collisional ionization is important, is excluded (dashed curve).

Figure 1. The turnover at $N_{\text{HI}} \lesssim 10^{13}$ cm^{-2} may thus be real and be caused by the turnover of the density distribution below the mean density. However, as discussed before, both the observations and the physical model are unreliable in this regime. The steepening at $N_{\text{HI}} \sim 10^{14.5}$ cm^{-2} reflects the fall-off in the density distribution due to the onset of rapid, non-linear collapse. Finally, the flattening at $N_{\text{HI}} \gtrsim 10^{16}$ cm^{-2} can be attributed to the flattening of the density distribution at $\delta \gtrsim 10^2$ due to the virialization of collapsed matter.

To show that the derived matter distribution is consistent with what would be expected from gravitational instability, the distribution of gas in a hydrodynamical simulation at $z = 2.75$ is indicated by the solid line in Figure 2. The simulation, which was kindly provided by T. Theuns, has the same cosmological parameters as were used to calculate the data points. It has the same ionization background as the simulation described in Schaye et al. (2000), and the temperature of the low-density gas agrees with the measurements of those authors. To compare the shape of the matter distribution functions, the simulation data has been shifted vertically so that it has the same maximum as the Hu et al. (1995) points.

The shape of the simulated matter distribution agrees fairly well with the distribution derived from the observations, although it seems to overpredict the mass fraction in the range $\delta \sim 10$ – 100 . Most of this excess can in fact be attributed to hot gas for which collisional ionization is important. This gas is much more highly ionized than cooler, photoionized gas of the same density and will therefore give rise to absorption lines of much lower column densities than predicted by equation 10. The dashed curve indicates the density distribution of gas cooler than $10^{4.8}$ K, a temperature sufficiently low for collisional ionization to be negligible. The agreement between this distribution and the points derived from the column density distribution of Petitjean et al. (1993) is remarkable.

The slope of the column density distribution over the range

$N_{HI} \sim 10^{13}-10^{14} \text{ cm}^{-2}$ is found to steepen from $z \sim 2$ to $z \sim 0$ (e.g., Davé & Tripp 2001; Penton, Shull, & Stocke 2000; Kim, Cristiani, & D’Odorico 2001; Weymann et al. 1998). If gravitational instability is responsible for the shape of the gas density distribution, then this distribution will be similar at $z \sim 0$ and $z \sim 3$, provided it is expressed as a function of the density relative to the cosmic mean. Hence, the change in the slope of the column density distribution must mainly be due to the evolution of the function $N_{HI}(\delta)$, which is determined by the expansion of the universe and the evolution of the ionizing background. Equation 10 shows that changes in z or Γ are equivalent to shifting the N_{HI} -axis (the upper x-axis) in Figure 2 relative to the $(1 + \delta)$ -axis (the lower x-axis).

In section 3.1 it was shown that the neutral hydrogen column density corresponding to a fixed density contrast is about a factor $5 \times 10^2 \Gamma(z=0)/\Gamma(z=3) \sim 5-50$ lower at $z \sim 0$ than at $z \sim 3$. At $z \sim 3$, the distribution is found to be steepest in the range $\log N_{HI} \sim 14.5-15.5$, which corresponds to $\delta \sim 5-25$. This same range in density contrast corresponds to $\log N_{HI} \sim 13.2-14.2$ at $z \sim 0$. Hence, the steepening of the slope of the column density distribution has the same origin at low and high redshift, it is caused by the fall-off in the probability distribution of the gas density at the onset of rapid, non-linear collapse. Similarly, one would expect the flattening observed at $\log N_{HI} \gtrsim 16$ at $z \sim 3$ to shift to $\log N_{HI} \gtrsim 15$ by $z \sim 0$, in agreement with the observations of Weymann et al. (1998).

5. CONCLUSIONS

In the last decade semi-analytic models and numerical simulations were used to show that the Ly α forest is produced naturally in cold dark matter models with initially scale invariant, adiabatic fluctuations. Low column density absorption lines are predicted to arise in the smoothly fluctuating, photoionized IGM, which contains a large fraction of the baryons in the universe. This paper demonstrates that this physical picture is in fact generic and can be derived using straightforward physical arguments, without making any specific assumptions about the cosmology, the presence and distribution of dark matter or the mechanism for structure formation.

The key physical argument is that the sound crossing time (t_{sc}) along any sightline intersecting a cloud, is in general of order the local dynamical time (t_{dyn}), regardless of the shape of the cloud and regardless of whether the cloud as a whole is in dynamical equilibrium. This argument holds if the characteristic size (the scale over which the density is of order the maximum density) is smaller than the sound horizon, which is true for overdense absorbers (except for a short period after reionization). If, for whatever reason, a large departure from local hydrostatic equilibrium occurs, then local equilibrium will be restored on a timescale $\min(t_{sc}, t_{dyn})$, which is much smaller than the Hubble time if the absorber is overdense and out of equilibrium. The only way to systematically violate the condition $t_{sc} \sim t_{dyn}$, is to postulate that all Ly α forest absorbers are pressure confined, a proposal that has been ruled out on both observational and theoretical grounds (e.g., Rauch 1998), that they are rotationally supported *and* that their spin axes are always nearly perpendicular to the line of sight, or that the fraction of baryons in quasi-stable ($t \sim t_{sc} \sim t_{dyn} < H^{-1}$) gas clouds is negligible compared with the fraction in transient ($t \sim \min(t_{sc}, t_{dyn}) \ll \max(t_{sc}, t_{dyn})$) clouds.

Using just the condition $t_{sc} \sim t_{dyn}$ and an estimate of the

temperature ($T \sim 10^4$ K) and ionization rate ($\Gamma \sim 10^{-12} \text{ s}^{-1}$ at $z \sim 3$), it was shown that unless the ratio of baryonic to collisionless matter is orders of magnitude lower than is generally assumed, the Ly α forest absorbers must be extended structures of low overdensity. Furthermore, the conclusion that the low column density absorbers contain a large fraction of the baryons, follows directly from the observed column density distribution.

Scaling relations were derived for the radial sizes and characteristic densities of the absorbers. It was shown that if the parameters of the model are set to the values appropriate for the specific model that was simulated by Davé et al. (1999), then the density - column density relation agrees very well with their empirical fitting formula. Finally, the mass-weighted probability distribution of the gas density was derived from the observed column density distribution. This led to several new insights: the shape of the column density distribution, in particular the deviations from a single power-law, and its evolution with redshift, reflect the shape of the matter distribution, which agrees remarkably well with the shape of the distribution produced by the growth of structure in an expanding universe via gravitational instability.

This work demonstrates that Jeans smoothing is central to the small-scale structure of the Ly α forest. It is therefore likely that studies in which the effect of gas pressure is neglected, or in which the Jeans length is varied only in time, are only reliable on scales greater than the sound horizon. On these scales ($\gg 10^2 \text{ km s}^{-1}$), gas pressure is unimportant and the gas should be a good tracer of the large-scale distribution of the matter.

It is important to note that the observational support for the current physical picture of the Ly α forest is much less strong for the high column density lines ($N_{HI} \gtrsim 10^{16} \text{ cm}^{-2}$) than it is for the low column density forest, which formed the main focus of this work. It is for example possible, perhaps even likely, that galactic winds affect some of the high-density gas that gives rise to the strong absorption lines (e.g., Theuns, Mo, & Schaye 2001).

Although the derived properties of the Ly α forest absorbers are not particularly sensitive to the presence of dark matter, dark matter may still be required to form the observed structure in the forest from the small-amplitude fluctuations ($\delta \sim 10^{-5}$) observed at $z \sim 10^3$ in the cosmic microwave background. Indeed, it is well-known that if gravitational instability is responsible for structure formation, then dark matter (or a modification of gravity) is required to grow the observed (non-linear) structure. Here, the shape of the matter distribution function was derived directly from the observed column density distribution using the analytic model, which does not make any assumptions about the mechanism for structure formation. The fact that the derived shape agrees with the expectations from gravitational instability in an expanding universe, lends credence to the use of ab-initio hydrodynamical simulations to investigate the detailed properties of the forest and their dependence on the parameters of the models.

I am grateful to Tom Theuns for giving me permission to use one of his simulations for figure 2. It is a pleasure to thank Anthony Aguirre, John Bahcall, Jordi Miralda-Escudé, and Eliot Quataert for discussions and a careful reading of the manuscript. This work was supported by a grant from the W. M. Keck Foundation.

REFERENCES

- Bechtold, J., Crots, A. P. S., Duncan, R. C., & Fang, Y. 1994, ApJ, 437, L83
 Bi, H. G., Börner, G., & Chu, Y. 1992, A&A, 266, 1
 Bryan, G. L., & Machacek, M. E. 2000, ApJ, 534, 57
 Bryan, G. L., Machacek, M., Anninos, P., & Norman, M. L. 1999, ApJ, 517, 13
 Carswell, R. F., Morton, D. C., Smith, M. G., Stockton, A. N., Turnshek, D. A., & Weymann, R. J. 1984, ApJ, 278, 486
 Cen, R., Miralda-Escudé, J., Ostriker, J. P., & Rauch, M. 1994, ApJ, 437, L9
 Croft, R. A. C., Weinberg, D. H., Katz, N., & Hernquist, L. 1998, ApJ, 495, 44
 Davé, R., & Tripp, T. M. 2001, ApJ, in press (astro-ph/0101419)
 Davé, R., Hernquist, L., Katz, N., & Weinberg, D. H. 1999, ApJ, 511, 521 (DHKW)
 Dinshaw, N., Impey, C. D., Foltz, C. B., Weymann, R. J., & Chaffee, F. H. 1994, ApJ, 437, L87
 Dinshaw, N., Foltz, C. B., Impey, C. D., Weymann, R. J., & Morris, S. L. 1995, Nature, 373, 223
 Efstathiou, G., Schaye, J., & Theuns, T. 2000, Philos. Trans. R. Soc. Lond. A, 358, 2049
 Gnedin, N. Y. 2000, ApJ, 542, 535
 Gnedin, N. Y., & Hui, L. 1998, MNRAS, 296, 44
 Haardt, F., & Madau, P. 1996, ApJ, 461, 20
 Hernquist, L., Katz, N., Weinberg, D. H., & Miralda-Escudé, J. 1996, ApJ, 457, L51
 Hu, E. M., Kim, T., Cowie, L. L., Songaila, A., & Rauch, M. 1995, AJ, 110, 1526
 Hui, L., & Gnedin, N. Y. 1997, MNRAS, 292, 27
 Kim, T.-S., Hu, E. M., Cowie, L. L., & Songaila, A. 1997, AJ, 114, 1
 Kim, T.-S., Cristiani, S., & D'Odorico, S. 2001, A&A, in press (astro-ph/0101005)
 Kirkman, D., & Tytler, D. 1997, ApJ, 484, 672
 McDonald, P., Miralda-Escudé, J., Rauch, M., Sargent, W. L. W., Barlow, T. A., & Cen, R. 2001, ApJ, submitted (astro-ph/0005553)
 Miralda-Escudé, J., Cen, R., Ostriker, J. P., & Rauch, M. 1996, ApJ, 471, 582
 Nusser, A., & Haehnelt, M. 1999, MNRAS, 303, 179
 O'Meara, J. M., Tytler, D., Kirkman, D., Suzuki, N., Prochaska, J. X., Lubin, D., & Wolfe, A. M. 2001, ApJ, 552, 718
 Penton, S. V., Shull, J. M., & Stocke, J. T. 2000, ApJ, 544, 150
 Petitjean, P., Webb, J. K., Rauch, M., Carswell, R. F., & Lanzetta, K. 1993, MNRAS, 262, 499
 Rauch, M., et al. 1997, ApJ, 489, 7
 Rauch, M. 1998, ARA&A, 36, 267
 Rees, M. J. 1986, MNRAS, 218, 25P
 Ricotti, M., Gnedin, N. Y., & Shull, J. M. 2000, ApJ, 534, 41
 Schaye, J., 2001, in preparation
 Schaye, J., Theuns, T., Leonard, A., & Efstathiou, G. 1999, MNRAS, 310, 57
 Schaye, J., Theuns, T., Rauch, M., Efstathiou, G., & Sargent, W. L. W. 2000, MNRAS, 318, 817
 Scott, J., Bechtold, J., Dobrzycki, A., & Kulkarni, V. P. 2000, ApJS, 130, 67
 Smette, A., Robertson, J. G., Shaver, P. A., Reimers, D., Wisotzki, L., & Köhler, T. 1995, A&AS, 113, 199
 Theuns, T., Leonard, A., Efstathiou, G., Pearce, F. R., & Thomas, P. A. 1998, MNRAS, 301, 478
 Theuns, T., Mo, H. J., & Schaye, J. 2001, MNRAS, 321, 450
 Tytler, D. 1987, ApJ, 321, 49
 Weinberg, D. H., Miralda-Escudé, J., Hernquist, L., & Katz, N. 1997, ApJ, 490, 564
 Weymann, R. J. et al. 1998, ApJ, 506, 1
 Zhang, Y., Anninos, P., & Norman, M. L. 1995, ApJ, 453, L57

APPENDIX

FULL EQUATIONS

In the equations appearing in the main text, numerical values were inserted for the natural constants, as well as for many other physical parameters. For reference, a list of the full expressions is listed below. The contributions to the gas and electron densities of elements other than hydrogen and helium are neglected.

Hydrodynamics

The dynamical timescale $t_{\text{dyn}} \equiv 1/\sqrt{G\rho}$ is

$$t_{\text{dyn}} = \sqrt{\frac{(1-Y)f_g}{Gm_H n_H}}. \quad (\text{A1})$$

The sound crossing timescale $t_{\text{sc}} \equiv L/c_s$ is

$$t_{\text{sc}} = L \sqrt{\frac{\mu m_H}{\gamma k T}}. \quad (\text{A2})$$

The condition $t_{\text{dyn}} = t_{\text{sc}}$ defines the Jeans length,

$$L_J = \left(\frac{\gamma k}{\mu m_H^2 G} \right)^{1/2} (1-Y)^{1/2} f_g^{1/2} n_H^{-1/2} T^{1/2}. \quad (\text{A3})$$

The gaseous Jeans mass $M_{g,J} \equiv \rho_g L_J^3$ is

$$M_{g,J} = \left(\frac{\gamma k}{\mu m_H^{4/3} G} \right)^{3/2} (1-Y)^{1/2} f_g^{3/2} n_H^{-1/2} T^{3/2}, \quad (\text{A4})$$

and the total Jeans mass is a factor $1/f_g$ greater. The Jeans column density in hydrogen $N_{H,J} \equiv n_H L_J$ is

$$N_{H,J} = \left(\frac{\gamma k}{\mu m_H^2 G} \right)^{1/2} (1-Y)^{1/2} f_g^{1/2} n_H^{1/2} T^{1/2}. \quad (\text{A5})$$

Equations valid for an optically thin plasma

The neutral fraction of a highly ionized, optically thin gas is

$$\frac{n_{HI}}{n_H} = n_H \frac{1-Y/2}{1-Y} \frac{\beta_{HI}}{\Gamma}. \quad (\text{A6})$$

Substituting this into the expression for the Jeans column density yields

$$N_{HI} = \left(\frac{\gamma k}{\mu m_H^2 G} \right)^{1/2} \frac{1-Y/2}{(1-Y)^{1/2}} f_g^{1/2} \beta_{HII} \Gamma^{-1} n_H^{3/2} T^{1/2}. \quad (\text{A7})$$

The hydrogen number density is related to the density contrast $\delta \equiv (\rho - \bar{\rho})/\bar{\rho}$,

$$n_H = \frac{3\Omega_b H_0^2}{8\pi G m_H} (1-Y)(1+z)^3 (1+\delta). \quad (\text{A8})$$

Using this relation, the neutral hydrogen column density can be expressed in terms of the density contrast,

$$N_{HI} = \left(\frac{3}{8\pi} \right)^{3/2} \left(\frac{\gamma k}{\mu m_H^2 G^4} \right)^{1/2} (1-Y)(1-Y/2)(\Omega_b H_0^2)^{3/2} (1+z)^{9/2} f_g^{1/2} \beta_{HII} \Gamma^{-1} T^{1/2} (1+\delta)^{1.5}. \quad (\text{A9})$$

Substituting equation A7 into equation A3 yields an expression relating the Jeans length to the neutral hydrogen column density,

$$L_J = \left(\frac{\gamma k}{\mu m_H^2 G} \right)^{2/3} [(1-Y)(1-Y/2)]^{1/3} f_g^{2/3} \beta_{HII}^{1/3} \Gamma^{-1/3} T^{2/3} N_{HI}^{-1/3}. \quad (\text{A10})$$

Similarly, by substituting equation A7 into equation A4 the gaseous Jeans mass can be expressed in terms of N_{HI} ,

$$M_{g,J} = \left(\frac{\gamma k}{\mu m_H^{7/5} G} \right)^{5/3} [(1-Y)(1-Y/2)]^{1/3} f_g^{5/3} \beta_{HII}^{1/3} \Gamma^{-1/3} T^{5/3} N_{HI}^{-1/3}, \quad (\text{A11})$$

and the total Jeans mass is again a factor $1/f_g$ greater. The density of neutral hydrogen relative to the critical density $\rho_c = \frac{3H_0^2}{8\pi G}$, can be obtained from the number density of absorption lines per unit absorption distance and column density, $f(N_{HI}, z)$ (see equation 15 for the definition of f),

$$\Omega_{HI} = \frac{8\pi G m_H}{3H_0 c} \int N_{HI} f(N_{HI}, z) dN_{HI}. \quad (\text{A12})$$

Using equations A6 and A7, this can be converted into an expression for the total gas density,

$$\Omega_g = \frac{8\pi}{3} \frac{1}{H_0 c} \left(\frac{\gamma k m_H G^2}{\mu} \right)^{1/3} [(1-Y)(1-Y/2)]^{-1/3} f_g^{1/3} \beta_{HII}^{-1/3} \Gamma^{1/3} T^{1/3} \int N_{HI}^{1/3} f(N_{HI}, z) dN_{HI}. \quad (\text{A13})$$

If the gas is not isothermal, then β_{HII} and T depend on N_{HI} and should be moved inside the integral.

Finally, the results derived in this paper are equally valid for the He II Ly α forest, provided that N_{HI} is replaced by N_{HeII} using

$$\frac{N_{HeII}}{N_{HI}} = \frac{Y}{4(1-Y)} \frac{\beta_{HeIII}}{\beta_{HII}} \frac{\Gamma_{HI}}{\Gamma_{HeII}}, \quad (\text{A14})$$

where $\beta_{HeIII}/\beta_{HII} \approx 5.3$.